

Ship Detection Using X-Bragg Scattering Model Based on Compact Polarimetric SAR



Chenghui Cao, Xingpeng Mao, Jie Zhang, Junmin Meng, Xi Zhang, and Genwang Liu

Abstract Compact polarimetric SAR is currently drawing more attention owing to its advantage in earth observations. In this paper, based on scattering vector in hybrid mode and X-Bragg scattering model, a new method is presented for evaluating ship detection performance. By using this method, three polarization features, including circular polarization ratio, relative phase, and roundness, were analyzed selectively. Experiments performed using hybrid mode emulated from C-band RADARSAT-2 full polarimetric SAR data validate the feasibility of the method in analyzing the ship detection performance.

Keywords Compact polarimetric SAR · Scattering model · Ship detection · Polarization features

This work was supported by the National Key R&D Program of China (2017YFC1405201), Public Science and Technology Research Funds Projects of Ocean (201505002), and the National Key R&D Program of China (2016YFC1401001).

C. Cao

Harbin Institute of Technology (HIT), Harbin, China

First Institute of Oceanography, Ministry of Natural Resources, Qingdao, China

X. Mao (✉)

Harbin Institute of Technology (HIT), Harbin, China

e-mail: mxp@hit.edu.cn

J. Zhang · J. Meng · X. Zhang · G. Liu

First Institute of Oceanography, Ministry of Natural Resources, Qingdao, China

e-mail: zhangjie@fio.org.cn; mengjm@fio.org.cn; xi.zhang@fio.org.cn; liugenwang@fio.org.cn

© Springer Nature Switzerland AG 2019

E. T. Quinto et al. (eds.), *The Proceedings of the International Conference on*

Sensing and Imaging, 2018, Lecture Notes in Electrical Engineering 606,

https://doi.org/10.1007/978-3-030-30825-4_8

1 Introduction

Ship surveillance is of great significance to ocean security and marine management [1]. The synthetic aperture radar (SAR), which can work day and night with high resolution, even under cloudy conditions, has been given great concern for ship detection over the past 30 years.

With the improvement of radar system and ship detection algorithms, the SAR data acquisition mode has been extended from single and dual polarimetric SAR to full polarimetric (FP) SAR [2]. Contrast with single and dual polarimetric SAR, FP SAR can provide more target information and allows complete backscattering characterization of scatterers [3]. However, the narrow swath width of FP SAR can't meet the application demands (*e.g.*, the maximum swath of radarsat-2 is just 50 km), which limits its development.

To solve the problem in FP SAR, compact polarimetric (CP) SAR appears with wide swath coverage and less energy budget [4–6], which has been widely studied, and a lot of promising results have been obtained [5–7]. According to the polarization state, three CP SAR modes have been proposed, including $\pi/4$ [8], dual circular polarization [9], and hybrid polarization (HP) [10]. Among which, the HP mode is simpler, more stable and less sensitive to noise than the other two modes. Furthermore, the HP mode achieves a better performance in self-calibration and engineering [11]. So far, the RISA-1 in India, the ALOS-2 in Japan, even the future Canadian RADARSAT Constellation Mission (RCM) all supports the HP mode, which is most suitable for marine applications.

Extracting effective polarization features from Stokes Vector can essentially reflect the physical difference between ships and sea clutter [6]. The feasibility of feature extraction was verified by researchers in a series of study. For example, Shirvany et al. [12] indicated the effectiveness of the degree of polarization (DoP) in ship detection. Then, this work was further studied by Touzi, who defined an excursion of the DoP to enhance a significant ship-sea contrast [13]. In contrasting with single polarimetric parameter, Yin investigated the capability of $m-\alpha$ and $m-\chi$ decompositions for ship detection [14]. Three features extracted from CP SAR were proved to have a good performance in ship detection [3]. What's more, Paes showed a more detailed analysis of the detection capability and sensitivity [15] of δ together with m , μ_C , $|\mu_{xy}|$, and entropy H_ω .

In summary, the existing polarization parameters from polarization decomposition are used directly without considering the influence of sea surface roughness, which weakens the detection capability of the polarization parameters to some extent. In this paper, a new method for analyzing the polarization parameters is presented by introducing the sea surface roughness disturbance [16]. In this case, the polarization parameters can be evaluated in both theory and experiments for ship detection.

Section 2 gives the formula derivation of the presented target scattering model, and the surface roughness of sea is introduced. In Sect. 3, the presented target scattering model is applied to analyze the polarization difference of circular

polarization ratio, roundness, and relative phase between ships and sea to prove its availability. Finally, in Sect. 4, the conclusion is given.

2 New Method for Feature Analysis

In hybrid mode, the radar antenna transmits a circular signal and simultaneously receives two orthogonal linear-polarization signals. Consider that radar transmits a right-circular signal, the scattering vector is [17]

$$\vec{k}_l = [E_{RH} \ E_{RV}]^T = \frac{1}{\sqrt{2}}(S_{HH} - jS_{HV}, -jS_{VV} + S_{HV})^T \quad (1)$$

As we know, the coherency matrix T is a 3×3 matrix [3] as follows:

$$T = \vec{k}_p \vec{k}_p^H = \begin{bmatrix} T_{11} & T_{12} & T_{13} \\ T_{21} & T_{22} & T_{23} \\ T_{31} & T_{32} & T_{33} \end{bmatrix} = \begin{bmatrix} 2A_0 & C - jD & H + jG \\ C + jD & B_0 + B & E + jF \\ H - jG & E - jF & B_0 - B \end{bmatrix} \quad (2)$$

where $\vec{k}_p = \frac{1}{\sqrt{2}}[S_{HH} + S_{VV} \ S_{HH} - S_{VV} \ 2S_{HV}]^T$, $A_0, B, B_0, C, D, E, F, G, H$ are Huynen parameters [18].

The matrix T_3 can be expressed by S_{HH}, S_{HV}, S_{VV} , which is extremely complicated. In this case, a new idea is proposed by using the elements of the scattering vector. We do the operation as

$$\begin{cases} E_{RH} + jE_{RV} = S_{HH} + S_{VV} \\ E_{RH} - jE_{RV} = S_{HH} - S_{VV} - 2jS_{HV} \end{cases} \quad (3)$$

Then a new matrix Y is defined consequently as

$$\begin{aligned} Y &= \begin{bmatrix} E_{RH} + jE_{RV} \\ E_{RH} - jE_{RV} \end{bmatrix} \begin{bmatrix} (E_{RH} + jE_{RV})^H & (E_{RH} - jE_{RV})^H \end{bmatrix} \\ &= \begin{bmatrix} S_{HH} + S_{VV} \\ S_{HH} - S_{VV} - 2jS_{HV} \end{bmatrix} \begin{bmatrix} (S_{HH} + S_{VV})^H & (S_{HH} - S_{VV} - 2jS_{HV})^H \end{bmatrix} \\ &= \begin{bmatrix} (S_{HH} + S_{VV})(S_{HH} + S_{VV})^* & (S_{HH} + S_{VV})(S_{HH} - S_{VV})^* + 2jS_{HV}^* \\ (S_{HH} - S_{VV} - 2jS_{HV})(S_{HH} + S_{VV})^* & (S_{HH} - S_{VV} - 2jS_{HV})(S_{HH} - S_{VV})^* + 2jS_{HV}^* \end{bmatrix} \end{aligned} \quad (4)$$

The matrix Y can be described by the coherency matrix T

$$Y = \begin{bmatrix} T_{11} & T_{12} + jT_{13} \\ T_{12}^* - jT_{13}^* & T_{22} + T_{33} - 2\text{Im}(T_{23}) \end{bmatrix} \quad (5)$$

By using Huynen parameters [18] the matrix Y is

$$Y = \begin{bmatrix} 2A_0 & (C - G) + j(H - D) \\ (C - G) - j(H - D) & 2(B_0 - F) \end{bmatrix} \quad (6)$$

In Wang et al. [18], the stokes vector of the scattered wave in hybrid mode is written as

$$g = \begin{bmatrix} g_0 \\ g_1 \\ g_2 \\ g_3 \end{bmatrix} = \begin{bmatrix} A_0 + B_0 - F \\ C - G \\ H - D \\ -A_0 + B_0 - F \end{bmatrix} \quad (7)$$

Hence, Y can be derived from Eqs. (5), (6), and (7) as

$$Y = \begin{bmatrix} T_{11} & T_{12} + jT_{13} \\ T_{12}^* - jT_{13}^* & T_{22} + T_{33} - 2\text{Im}(T_{23}) \end{bmatrix} \\ = \begin{bmatrix} g_0 - g_3 & g_1 + jg_2 \\ g_1 - jg_2 & g_0 + g_3 \end{bmatrix} \quad (8)$$

As a result, the stokes vector can be derived as

$$\begin{cases} g_0 = \frac{T_{11} + T_{22} + T_{33}}{2} - \text{Im}(T_{23}) \\ g_1 = \text{Re}(T_{12}) - \text{Im}(T_{13}) \\ g_2 = \text{Im}(T_{12}) + \text{Re}(T_{13}) \\ g_3 = \frac{-T_{11} + T_{22} + T_{33}}{2} - \text{Im}(T_{23}) \end{cases} \quad (9)$$

Based on the theory mentioned above, the coherency matrix T and stokes vector are used to represent the constructed matrix Y . For better description of the matrix Y , X-Bragg scattering model is introduced below.

X-Bragg scattering model is first introduced by Hajnsek et al. [16] in order to solve the case of nonzero cross-polarized backscattering and depolarization. By assuming a roughness disturbance induced random surface slope β , the X-Bragg scattering is modeled as a reflection depolarizer [16] as shown in Eq. (10).

$$T_{\text{X-Bragg}} = \begin{bmatrix} T_{11} & T_{12} & T_{13} \\ T_{21} & T_{22} & T_{23} \\ T_{31} & T_{32} & T_{33} \end{bmatrix} = \begin{bmatrix} C_1 & C_2 \sin c(2\beta_1) & 0 \\ C_2 \sin c(2\beta_1) & C_3(1 + \sin c(4\beta_1)) & 0 \\ 0 & 0 & C_3(1 - \sin c(4\beta_1)) \end{bmatrix} \quad (10)$$

where

$$\begin{cases} C_1 = |R_S + R_P|^2 \\ C_2 = (R_S + R_P)(R_S^* - R_P^*) \\ C_3 = \frac{1}{2}|R_S - R_P|^2 \end{cases}$$

β is assumed to follow a uniform distribution in the interval $[-\beta_1, \beta_1]$, and $\beta_1 < \pi/2$ is the distribution width.

Combined with Eqs. (9) and (10), the stokes vector can be described by X-Bragg scattering matrix as

$$\begin{cases} g_0 = \frac{T_{11}+T_{22}+T_{33}}{2} - \text{Im}(T_{23}) = \frac{C_1+2C_3}{2} \\ g_1 = \text{Re}(T_{12}) - \text{Im}(T_{13}) = \text{Re}(C_2 \sin c(2\beta_1)) \\ g_2 = \text{Im}(T_{12}) + \text{Re}(T_{13}) = \text{Im}(C_2 \sin c(2\beta_1)) \\ g_3 = \frac{-T_{11}+T_{22}+T_{33}}{2} - \text{Im}(T_{23}) = \frac{-C_1+2C_3}{2} \end{cases} \quad (11)$$

With the analysis of scattering difference of ships and sea, Eq. (11) can evaluate the performance of the polarization features in ship detection.

3 Ship Detection Performance Analysis

According to the target scattering model of ships in Sect. 2, the polarization parameters, such as, circular polarization ratio, roundness, and relative phase, which have good performance in ship detection [19], are analyzed for example to extract new parameter. For lack of compact polarimetric SAR data, full polarimetric RADARSAT-2 SAR data are chosen to reconstruct the compact polarimetric SAR data transmitted by right-circular polarization and received by horizontal and vertical polarization. Note that the formulas are

$$\text{CPR} = \frac{g_0 - g_3}{g_0 + g_3}, \quad \sin 2\chi = -\frac{g_3}{\sqrt{g_1^2 + g_2^2 + g_3^2}}, \quad \delta = \tan^{-1}\left(\frac{g_3}{g_2}\right) \quad (12)$$

Circular Polarization Ratio

The circular polarization ratio (CPR) is derived from Eqs. (11) and (12) as

$$\text{CPR} = \frac{C_1}{2C_3} = \frac{|R_S + R_P|^2}{|R_S - R_P|^2} = \frac{|S_{HH} + S_{VV}|^2}{|S_{HH} - S_{VV}|^2} \quad (13)$$

In Eq. (13), the value of the CPR is positive, which is only related to the dielectric constant and the incidence angle, and is independent of the rotation angle. Therefore, this parameter is stable and can be used in ship detection.

Figure 1 is a part of SAR image, which shows the value of CPR about ships and sea. We can see the value of the ship is basically between 0 and 1, while the value of the sea surface is greater than 1. Hence, the ships and sea surface can be separated

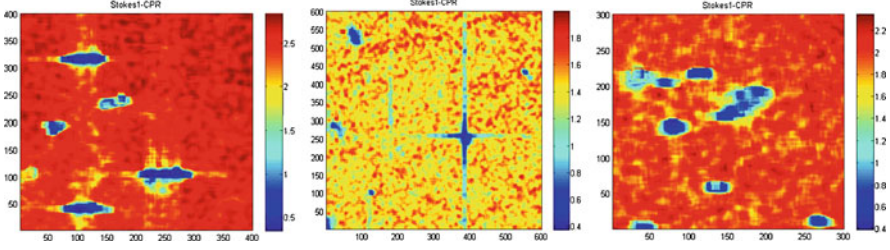


Fig. 1 Value of circular polarization ratio about the ships and sea surface

by the threshold 1. However, the value of CPR in the figure ranges from 0.4 to 2.5, which means the span is too small to select the threshold properly.

Roundness

Roundness can be derived from Eqs. (11) and (12) as

$$\sin 2\chi = \frac{C_1 - 2C_3}{\sqrt{4(C_2 \sin c(2\beta_1))^2 + (-C_1 + 2C_3)^2}} \quad (14)$$

In Eq. (14), the value of χ and $\sin 2\chi$ is consistent whether it is positive or negative. On the right side of the Eq. (14), the denominator is positive, so the positive and negative properties of χ depends on the numerator. Assuming that the phase angle of $S_{HH}S_{VV}^*$ is θ_{HH-VV} , the numerator is derived as

$$C_1 - 2C_3 = 2 \operatorname{Re}(S_{HH}S_{VV}^*) = 2 \cos(\theta_{HH-VV}) \quad (15)$$

According to Eq. (15), the denominator on the right side is positive, as a result, the value of $C_1 - 2C_2$ is decided by the phase angle θ_{HH-VV} . We know that the initial value of the phase angle is $\pi/2$, and with each additional scattering, the phase angle increases π . Therefore, the phase angles are $3\pi/2$ and $5\pi/2$ for single scattering and even scattering respectively. Consequently, for single scattering, the value of $\cos(\theta_{HH-VV})$ is positive, while for even scattering, the value is negative.

The scattering of sea surface is mostly surface scattering, and the ship is mostly even scattering, so the value of sea surface should be positive and the ship should be negative. As is shown in Fig. 2, the ships and sea surface can be separated by the threshold 0. Notice that the value of roundness is related to the rotation angle, which is not stable in high sea conditions.

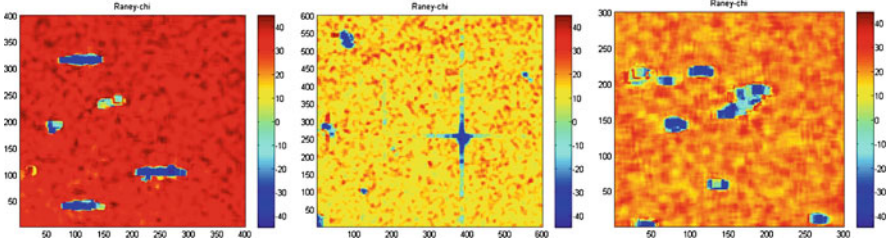


Fig. 2 Value of roundness about the ships and sea surface

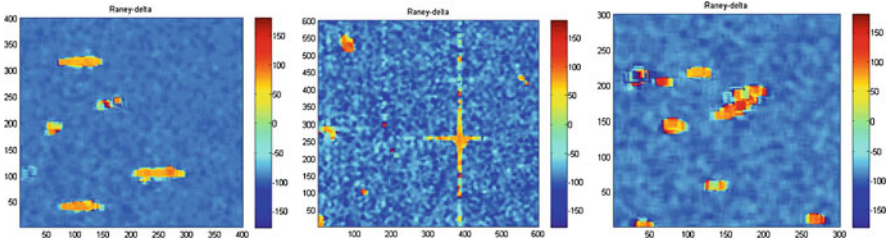


Fig. 3 Value of relative phase about the ships and sea surface

Relative Phase

Relative phase is derived from Eqs. (11) and (12) as

$$\delta = -\frac{1}{\sin c(2\beta_1)} \cot(\theta_{\text{HH-VV}}) \quad (16)$$

In Eq. (16), for single scattering, the phase angle is $3\pi/2$, so the value of $\cot(\theta_{\text{HH-VV}})$ is positive, which means the value of δ is negative. While for even scattering, the value of δ is positive. Due to different scattering characteristics, the ships in SAR image is mainly even scattering, while the sea surface is mainly surface scattering of ships and sea surface. Therefore, the value of the ships should be positive and the sea surface should be negative. An example is shown in Fig. 3, and the threshold 0 can be used to separate the ships and sea surface.

Note that the value of δ is related to the angle β in Eq. (16), the surface roughness increases with the increasing sea conditions. Therefore, the value of δ is unstable influenced by β , which is difficult to distinguish ships and the sea surface, especially in high sea conditions.

Figures 4 and 5 are experiments' results: (a) is the amplitude of RV polarization, and (b), (c), and (d) are results of threshold segmentation (the threshold are 1, 0 and 0). The areas with white are ships while dark and gray are sea surface. It indicates that the three features are all good discriminators for observing ships from sea surface. According to the scattering intensity, ships in Fig. 5 are bigger than

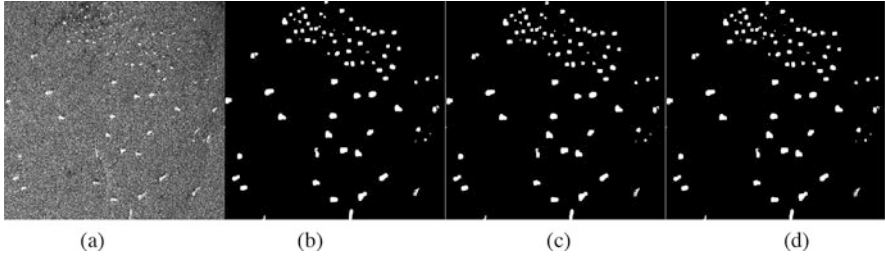


Fig. 4 Results of threshold segmentation. (a) RV image (b) CPR (c) Roundness (d) Relative phase

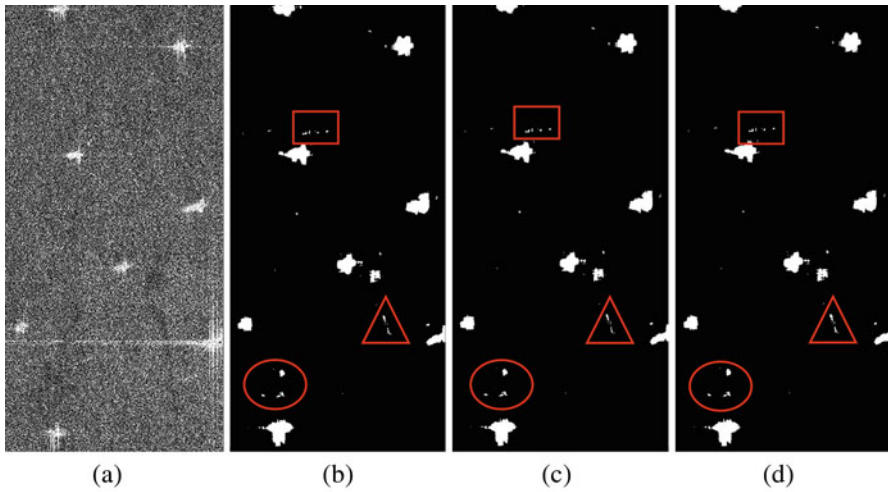


Fig. 5 Results of threshold segmentation. (a) RV image (b) CPR (c) Roundness (d) Relative phase

ships in Fig. 4. Combined with AIS, false alarms circled by red box are apparently owing to the high sea condition in Fig. 5. All in all, roundness and relative phase are all unstable in high sea conditions, while for CPR, the proper threshold is hard to choose in ship detection. The total number of detected ships is 166, and the false alarm rate of CPR, roundness, and relative phase are 0.06, 0.078, and 0.083, respectively.

4 Conclusion

In this paper, a new method of analyzing polarization parameter is derived by introducing the surface roughness of the sea. Three compact polarimetric parameters in hybrid mode are analyzed. The circular polarization ratio, roundness, and relative

phase can all be used to separate ships from sea surface. The circular polarization ratio is stable, but the span value is too small to select proper threshold for ship detection. Roundness and relative phase are not stable owing to their relation with rotation angle β , which increases the difficulty of ship detection, especially in high sea conditions. The false alarm rate of CPR, roundness, and relative phase are 0.06, 0.078, and 0.083, respectively by detecting 166 ships.

References

1. Ouchi, K. (2016). Current status on vessel detection and classification by synthetic aperture radar for maritime security and safety (pp. 5–12). In *Proceedings of Symposium on Remote Sensing of Environmental Sciences*, Gamagori, Japan, 2016.
2. Gao, G., Gao, S., He, J., et al. (2018). Adaptive ship detection in hybrid-polarimetric SAR images based on the power-entropy decomposition. *IEEE Transactions on Geoscience & Remote Sensing*, 99, 1–14.
3. Yin, J., Yang, J., Zhou, Z. S., et al. (2015). The extended bragg scattering model-based method for ship and oil-spill observation using compact polarimetric SAR. *IEEE Journal of Selected Topics in Applied Earth Observations & Remote Sensing*, 8(8), 3760–3772.
4. Souyris, J. C., & Sandra, M. (2002). Polarimetry based on one transmitting and two receiving polarizations: the $\pi/4$ mode (pp. 629–631). In *2002 IEEE International Geoscience and Remote Sensing Symposium, IGARSS'02*, 2002.
5. Charbonneau, F. J., Brisco, B., Raney, R. K., et al. (2010). Compact polarimetry overview and applications assessment. *Canadian Journal of Remote Sensing*, 36(Suppl 2), S298–S315.
6. Raney, R. K. (2006). Dual-polarized SAR and stokes parameters. *IEEE Geoscience and Remote Sensing Letters*, 3(3), 317–319.
7. Ouchi, K. (2013). Recent trend and advance of synthetic aperture radar with selected topics. *Remote Sensing*, 5(2), 716–807.
8. Souyris, J. C., Imbo, P., Fjortoft, R., et al. (2005). Compact polarimetry based on symmetry properties of geophysical media: The $\pi/4$ mode. *IEEE Transactions on Geoscience and Remote Sensing*, 43(3), 634–646.
9. Stacy, N., & Preiss, M. (2006). Compact polarimetric analysis of X-band SAR data (p. 6). In *Proceeding of EUSAR*, 2006.
10. Raney, R. K. (2007). Hybrid-polarity SAR architecture. *IEEE Transactions on Geoscience and Remote Sensing*, 45(11), 3397–3404.
11. Gao, G., Gao, S., He, J., et al. (2018). Ship detection using compact polarimetric SAR Based on the notch filter. *IEEE Transactions on Geoscience & Remote Sensing*, 99, 1–14.
12. Shirvany, R., Chabert, M., & Tourneret, J. Y. (2012). Ship and oil-spill detection using the degree of polarization in linear and hybrid/compact dual-pol SAR. *IEEE Journal of Selected Topics in Applied Earth Observations and Remote Sensing*, 5(3), 885–892.
13. Touzi, R., & Vachon, P. W. (2015). RCM polarimetric SAR for enhanced ship detection and classification. *Canadian Journal of Remote Sensing*, 41(5), 473–484.
14. Yin, J., & Yang, J. (2014). Ship detection by using the M-Chi and M-Delta decompositions (pp. 2738–2741). In *Geoscience and Remote Sensing Symposium. IEEE*, 2014.
15. Paes, R. L., Nunziata, F., & Migliaccio, M. (2016). On the capability of hybrid-polarity features to observe metallic targets at sea. *IEEE Journal of Oceanic Engineering*, 41(2), 346–361.
16. Hajnsek, I., Pottier, E., & Cloude, S. R. (2003). Inversion of surface parameters from polarimetric SAR[J]. *IEEE Transactions on Geoscience and Remote Sensing*, 41(4), 727–744.

17. Cloude, S. R., Goodenough, D. G., & Chen, H. (2012). Compact decomposition theory. *IEEE Geoscience and Remote Sensing Letters*, 9(1), 28–32.
18. Wang, H., Zhou, Z., Turnbull, J., et al. (2015). Three-component decomposition based on stokes vector for compact polarimetric SAR. *Sensors*, 15(9), 24087–24108.
19. Cao, C.-H., Zhang, J., Zhang, X., et al. (2017). The analysis of ship target detection performance with C band compact polarimetric SAR. *Periodical of Ocean University of China*, 47(2), 85–93.